Cellular and Molecular Bioengineering, Vol. 10, No. 5, October 2017 (© 2017) pp. 357–370
DOI: 10.1007/s12195-017-0486-7

Immunotheranostic Polymersomes Modularly Assembled from Tetrablock and Diblock Copolymers with Oxidation-Responsive Fluorescence

Fanfan Du,[1,4] Yu-Gang Liu,[1] and Evan Alexander Scott[1,2,3,4,5]

[1]Department of Biomedical Engineering, Northwestern University, Evanston, IL, USA; [2]Chemistry of Life Processes Institute, Northwestern University, Evanston, IL, USA; [3]Interdisciplinary Biological Sciences Program, Northwestern University, Evanston, IL, USA; [4]Simpson Querrey Institute, Northwestern University Feinberg School of Medicine, Chicago, IL, USA; and [5]Robert H. Lurie Comprehensive Cancer Center, Northwestern University Feinberg School of Medicine, Chicago, IL, USA

(*Received 16 February 2017; accepted 28 March 2017; published online 10 April 2017*)

Associate Editor Michael R. King oversaw the review of this article.

Abstract

Introduction—Intracellular delivery is a key step for many applications in medicine and for investigations into cellular function. This is particularly true for immunotherapy, which often requires controlled delivery of antigen and adjuvants to the cytoplasm of immune cells. Due to the complex responses generated by the stimulation of diverse immune cell populations, it is critical to monitor which cells are targeted during treatment. To address this issue, we have engineered an immunotheranostic polymersome delivery system that fluorescently marks immune cells following intracellular delivery.

Methods—Amine functionalized poly(ethylene glycol)-*bl*-poly(propylene sulfide) (PEG-PPS-NH_2) was synthesized by anionic ring opening polymerization and bridged *via* perylene bisimide (PBI) to form a tetrablock copolymer (PEG-PPS-PBI-PPS-PEG). Block copolymers were assembled into polymersomes by thin film hydration in phosphate buffered saline and characterized by dynamic light scattering, cryogenic electron microscopy and fluorescence spectroscopy. Polymersomes were injected subcutaneously into the backs of mice, and draining lymph nodes were extracted for flow cytometric analysis of cellular uptake and disassembly.

Results—Modular self-assembly of tetrablock/diblock copolymers in aqueous solutions induced π–π stacking of the PBI linker that both red-shifted and quenched the PBI fluorescence. Reactive oxygen species within the endosomes of phagocytic immune cell populations oxidized the PPS blocks, which disassembled the polymersomes for dequenching and shifting of the PBI fluorescence from 640 to 550 nm emission. Lymph node resident macrophages and dendritic cells were found to increase in 550 nm emission over the course of 3 days by flow cytometry.

Conclusions—Immunotheranostic polymersomes present a versatile platform to probe the contributions of specific cell populations during the elicitation of controlled immune responses. Flanking PBI with two oxidation-sensitive hydrophobic PPS blocks enhanced π stacking and introduced a mechanism for disrupting π–π interactions to shift PBI fluorescence in response to oxidative conditions. Shifts from red (640 nm) to green (550 nm) fluorescence occurred in the presence of physiologically relevant concentrations of reactive oxygen species and could be observed within phagocytic cells both *in vitro* and *in vivo*.

Address correspondence to Evan Alexander Scott, Department of Biomedical Engineering, Northwestern University, Evanston, IL, USA. Electronic mail: evan.scott@northwestern.edu

Evan Alexander Scott completed his undergraduate degree in Biomedical Engineering at Brown University in 2002. After working for a year as a chemical and biological defense engineer at the Battelle Memorial Institute in Aberdeen MD, he obtained a Ph.D. in Biomedical Engineering in 2009 from Washington University in St. Louis. His dissertation work was performed in the laboratory of Prof. Donald Elbert, where he developed methods based in proteomics and polymer chemistry to both analyze and control the interactions between blood and the material surfaces of cardiovascular devices. As a Whitaker International Scholar, he performed postdoctoral research in Switzerland in the laboratories of Prof. Jeffrey Hubbell and Prof. Melody Swartz at the École Polytechnique Fédérale de Lausanne (EPFL) from 2009 to 2013. There he focused on the development of nanomaterial-based formulations and strategies for both neonatal vaccination and cancer immunotherapy. Dr. Scott joined Northwestern University as a tenure-track Assistant Professor of Biomedical Engineering in the fall of 2013. His immunoengineering laboratory applies principles from biomaterials science, nanotechnology and tissue engineering towards the development of translational immunotherapies for heart disease and the rational design of vaccines for cancer and infectious diseases.

This paper is part of the 2017 Young Innovators Issue.

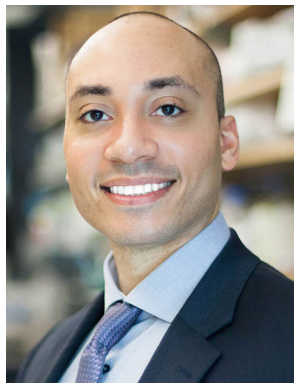

Keywords—Polymersome, Fluorescence, Theranostics, Perylene, Macrophage, Dendritic cell.

ABBREVIATIONS

APCs	Antigen presenting cells
CryoTEM	Cryogenic transmission electron microscopy
DCs	Dendritic cells
DLS	Dynamic light scattering
FBS	Fetal bovine serum
GPC	Gel permeation chromatography
MHCI	Major histocompatibility complex I
MW	Molecular weight
NK	Natural killer
PBI	Perylene bisimides
PTCDA	Perylene-3,4,9,10-tetracarboxylic dianhydride
PBS	Phosphate-buffered saline
PDI	Polydispersity index
PEG-*bl*-PPS	Poly(ethylene glycol)-*bl*-poly(propylene sulfide)
PITC	Polymer-bound isothiocyanate
ROS	Reactive oxygen species
SC	Subcutaneous
TLRs	Toll like receptors

INTRODUCTION

Theranostic strategies combine the ability of nanocarriers to package and transport both therapeutic and diagnostic payloads for simultaneous treatment of disease and assessment of targeted cells and tissues. Such methods have proved useful for understanding the mechanisms of action and sources of off-target effects for nanotherapies and have expanded the capabilities of diagnostic imaging techniques such as magnetic resonance imaging (MRI) and positron emission tomography (PET).[20,26] Personalized medicine may benefit extensively from the continued development of theranostic nanocarrier formulations by providing real time and individual assessment of therapeutic regimens. This is particularly true in the areas of cancer and immunotherapy, where variability between tumors and patient-specific immune history can significantly impact clinical outcomes of treatment.[8,32,33]

Here, we present an immunotheranostic (i.e., combining immunotherapy and diagnostics) platform, which specifically assesses nanocarrier targeting and intracellular disassembly within key cell populations that are critical to the initiation and understanding of immune responses. The balance between the oxidative and reductive potential within the endosomes of phagocytic cells is highly dependent on the specific cell subset and pathway of endocytosis.[34] Phagocytes are primarily comprised of neutrophils, macrophages and dendritic cells (DCs), the latter two being essential antigen presenting cells (APCs) that process foreign molecules for presentation to and activation of T cells. In addition to their innate immune functions, macrophages are essential scavengers that remove and destroy foreign pathogens and dead cells. To carry out these activities, macrophages trigger a respiratory burst during phagocytosis, rapidly generating reactive oxygen species (ROS) mainly at the plasma membrane.[2,44] Rapid degradation of engulfed materials is further enhanced by massive recruitment of V-ATPase, which acidifies their phagosomes within minutes to activate a host of proteolytic enzymes.[27,28] DCs on the contrary, demonstrate a more subtle oxidation within their phagosomes over the course of several hours and a lower potency for degradation relative to macrophages.[7,24] Sustained low levels of ROS during this time result in a gentler proteolysis that has been linked to their ability to generate the larger peptides required for MHCI presentation and enhanced cross presentation.[35] Furthermore, both macrophages and DCs express a wide range of phagocytic surface receptors that can route antigen into heterogeneous endosomal pathways with distinct mechanisms of degradation and antigen presentation.[1,6,13] In the case of DCs, activation of specific innate receptors, such as toll like receptors (TLRs), can significantly increase the oxidative and proteolytic capacity of their phagosomes.[3,40] Diagnostic methods that allow identification and mapping of how phagocytes are processing nanomaterials can therefore aid in understanding the complexity of the elicited immune responses.

Cell-dependent endosomal oxidation for enhanced MHCI presentation by dendritic cells has been previously achieved using poly(ethylene glycol)-*bl*-poly(propylene sulfide) (PEG-*bl*-PPS) copolymers. PEG-*bl*-PPS block copolymers are versatile redox-sensitive amphiphiles amenable to a diverse range of methods for self-assembly and characterization.[30,36,38] The molecular weight (MW) ratio of the hydrophilic PEG to hydrophobic PPS components can be specified by either ring-opening living polymerization or reversible addition-fragmentation chain-transfer polymerization.[14,30,36,38] The hydrophobic PPS block initiates the self-assembly and is responsible for aggregate stability, providing a critical micelle concentration bellow 10^{-7} M.[31] Depending on the individual block lengths, these copolymers can be engineered into a variety of different nanostructures, including solid-core spherical micelles (PEG_{44}-*bl*-

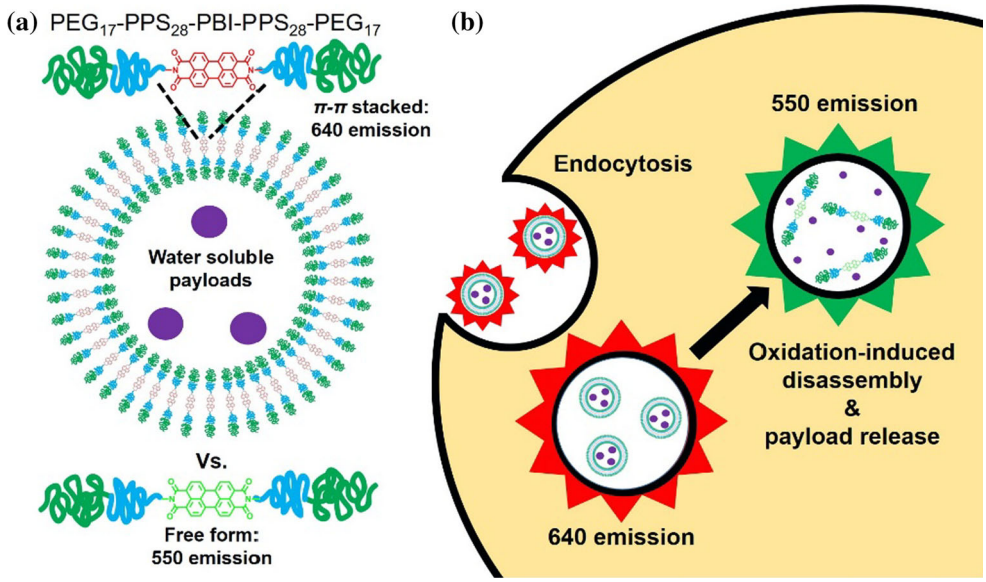

FIGURE 1. Schematic illustrations of (a) polymersomes encapsulating water soluble payloads formed from PEG_{17}-PPS_{28}-PBI-PPS_{28}-PEG_{17} tetrablock copolymers, and (b) their uptake and degradation by phagocytes. PEG_{17}-PPS_{28} copolymers were bridged by perylene bisimide (PBI), a hydrophobic dye that emits a red fluorescence when π-stacked within self-assembled membranes. Following endocytosis, disassembly of polymersomes by phagosomal reactive oxygen species (ROS) and pH-activated enzymes disrupts π–π stacking to shift the PBI emission spectrum to a green fluorescence.

PPS_{29}, MCs), vesicular polymersomes (PEG_{17}-*bl*-PPS_{30}, PSs), and cylindrical filomicelles (PEG_{45}-*bl*-PPS_{44}, FMs).[4,36–38,45] Each nanostructure achieves a distinct biodistribution and accommodates the loading of small molecules, biologics, fluorophores and contrast agents for multimodality imaging.[9,37,38] The polymersome morphology is particularly versatile in that both hydrophobic and hydrophilic payloads can be retained within its lipophilic membrane and aqueous lumen, respectively, for diverse theranostic and imaging strategies.[9,37,38,45] This permits incorporation of redox- and photo-sensitive mechanisms of degradation to promote spatiotemporally controlled intracellular delivery of antigen and immunostimulatory adjuvants of diverse solubilities and chemical properties.[9,30,36,38] In addition to block length, the nanostructure morphology can also be determined by the method of assembly. Several different methods are available for controlled assembly of PEG-*bl*-PPS, including solvent extraction and thin film hydration.[31,36] PEG-*bl*-PPS is non-immunogenic, allowing our nanocarriers to function as "blank slates" with an immunostimulatory potential based solely upon the selected molecules loaded inside.[36] PEG-*bl*-PPS block copolymers are therefore a unique tool for designing and engineering immunotheranostic delivery systems and incorporation of an innate sensor of disassembly into the copolymer chemistry could further enhance these capabilities.

Perylene bisimides (PBI) have been utilized as fluorescent dyes for a wide range of applications owing to their high quantum yield and photostability.[15,16,29,42] In biology, their chemical stability and low toxicity have proven advantageous for conjugation to nanomaterial probes and delivery systems.[10,42] The ability of these dyes to undergo π–π stacking has been employed for both supramolecular self-assembly and switchable concentration-dependent fluorescence emission.[5] Packing of PBI molecules has been well documented, with crystal structures of the investigated dyes exhibiting planar geometry and stacked into a parallel orientation at a distance between 3.34 and 3.55 Å.[21,42] This stacking has proven advantageous for supramolecular self-assembly of PBI-based nanoparticles.[22,23,42] Although free form solubilized PBI can generate green channel fluorescence, weakly interacting π-stacked PBI molecules can be excited to generate red emissions while stacking within aggregated PBI quenches emissions.[10,19,42,43] A red shift can be observed due to energy transfer to low-energy sites in packed PBI moieties.[46] Here, we use a perylene dianhydride to bridge two PEG-*bl*-PPS diblocks for the synthesis of a PEG-PPS-PBI-PPS-PEG tetrablock of the appropriate block lengths for polymersome assembly in aqueous solution. Spectral changes due to π–π stacking were used to generate oxidation switchable fluorescence for identification of PEG-*bl*-PPS polymersome intracellular disassembly (Fig. 1). Weak π–π stacking was pro-

moted within assemblies to provide a detectable red emission at 640 nm, and disassembly was detected by green emissions generated by free form solubilized tetrablock at 550 nm. *In vivo* degradation of PEG-PPS-PBI-PPS-PEG polymersomes within lymph node-resident phagocytes was observed following subcutaneous (SC) injection into mice.

MATERIALS AND METHODS

Materials

All reagents and solvents were obtained from commercial sources and used as received without further purification. *N*-(3-bromopropyl)phthalimide end-capped PEG-PPS block copolymers (PEG-PPS-PI) were synthesized by anionic ring opening polymerization of propylene sulfide, initiated by PEG thioacetate and terminated by addition of *N*-(3-bromopropyl)phthalimide, as previously described.[4] The removal of the phthaloyl group from PEG-PPS-PI to form amino end-functionalized PEG-PPS block copolymer (PEG-PPS-NH_2) was accomplished following a previously described method.[4] Polymer-bound isothiocyanate (PITC, 100–200 mesh, extent of labeling: 1.0–2.0 mmol/g loading, 1% crosslinked with divinylbenzene) and perylene-3,4,9,10-tetracarboxylic dianhydride (PTCDA) were purchased from Aldrich.

Synthesis of PEG_{17}-PPS_{28}-PBI-PPS_{28}-PEG_{17}

Perylene bisimide-bridged amphiphilic block copolymers PEG-PPS-PBI-PPS-PEG were synthesized by reaction of PTCDA with PEG-PPS-NH_2 (Scheme 1). PTCDA (80 g, 0.2 mmol), PEG_{17}-PPS_{28}-NH_2 (1.2 g, ~0.4 mmol) and pyridine (20 mL) were placed into a 35-mL pressure tube containing a magnetic stirring bar. The sealed reaction mixture was heated with stirring in an oil bath at 150 °C for 50 h. As the mixture cooled, 0.4 g of PITC was added and the mixture was stirred overnight at room temperature. After diluting the mixture with 30 mL of tetrahydrofuran, the solution was first filtered with filter paper and then filtered again with a 200 nm nylon membrane. The filtrate was concentrated and precipitated in cold diethyl ether to yield 0.66 g of PEG_{17}-PPS_{28}-PBI-PPS_{28}-PEG_{17}. Purity was verified by gel permeation chromatography (GPC) using Waters Styragel THF columns with a tetrahydrofuran mobile phase (0.6 mL/min) *via* both refractive index and UV/vis detectors (ThermoFisher Scientific). Structure was characterized by ^{1}H NMR on a Bruker-400 NMR spectrometer (400 MHz) using tetramethylsilane as an internal standard. ^{1}H NMR in $CDCl_3$: δ (ppm) = 8.69-8.66 (d, CH_{aromat}, PBI), 3.81–3.43 (m, CH_2, PEG), 3.36 (s, OCH_3, PEG), 3.06–2.83 (m, CH_2, PPS), 2.68–2.55 (m, CH, PPS), 1.39–1.30 (m, CH_3, PPS).

Polymersome Preparation and Characterization

Polymersomes were formed by the self-assembly of PEG_{17}-PPS_{28}-PBI-PPS_{28}-PEG_{17}/PEG_{17}-PPS_{28} (1/1 molar ratio) using the thin-film hydration method as previously described.[36,38,45] Briefly, 50 mg of block copolymer was dissolved in 0.5 mL dichloromethane within a 1.8 mL clear glass vial. After desiccation to remove the solvent, the resulting thin films were hydrated in 1.0 mL of phosphate-buffered saline (PBS) under shaking at 1500 rpm overnight. Single-layer polymersomes were obtained by extrusion through a 200 nm nylon membrane. The size distribution and zeta potential of the polymersomes were analyzed by dynamic light scattering (DLS) using Zetasizer Nano (Malvern Instruments) with a 4 mW He−Ne 633 nm laser at 1 mg/mL in PBS. The polydispersity index (PDI) was calculated using a two-parameter fit to the DLS correlation data. The morphology was determined by cryogenic transmission electron microscopy (cryoTEM).

Cell Culture

Cells from the murine macrophage cell line RAW 264.7 were obtained from the American Type Culture Collection (ATCC, Rockville, MD, USA) and cultured in RPMI 1640 medium supplemented with 10% fetal bovine serum (FBS), 100 IU/mL penicillin and 100 μg/mL streptomycin in 5% CO_2, 95% air and humidified atmosphere at 37 °C.

MTT Assay for Cell Viability

RAW 264.7 cells were seeded with 3000 cells in 100 μL for each well of a 96-well plate. 10 μL of polymersomes at various concentrations (0, 1, 5, 10, 20, and 50 mg/mL in PBS, respectively) was added. After incubation for 48 h, 10 μL of 5 mg/mL MTT was added, then incubated for another 4 h. Samples were washed twice with PBS and 200 μL of dimethylsulfoxide was added into each well to dissolve formazan that precipitated on the plate. The cell viability was calculated according to the absorbance determined using a microplate reader at 570 nm.

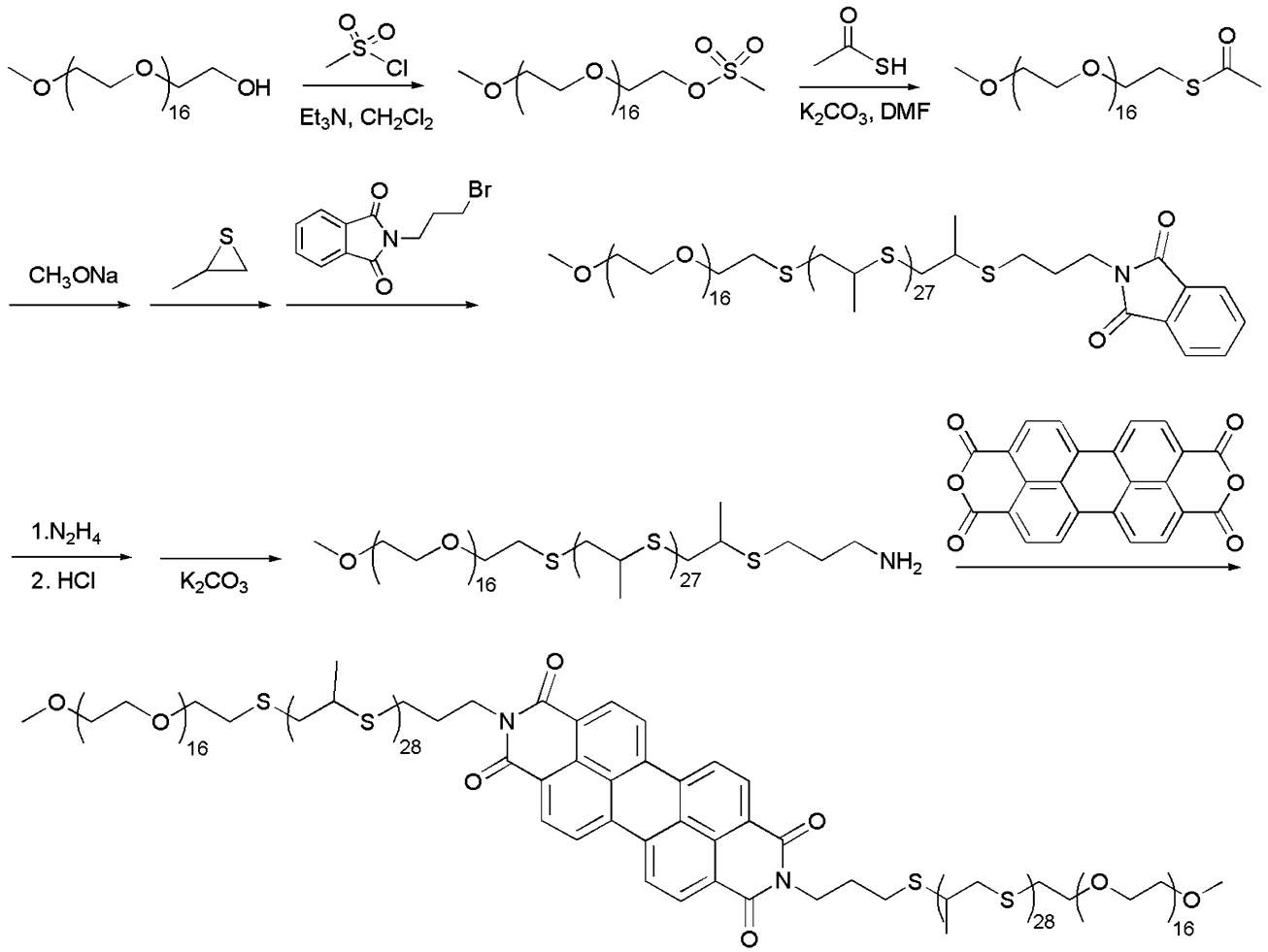

SCHEME 1. Synthesis of PEG_{17}-PPS_{28}-PBI-PPS_{28}-PEG_{17} tetrablock copolymer.

Cellular Uptake

RAW 264.7 cells were seeded in 1 mL of medium on a 12-well plate at 2×10^5 cells per well and cultured for 24 h. 20 μL of polymersomes with different concentrations (0, 5, 10, and 25 mg/mL in PBS, respectively) were added for each well. After incubation for 3 h, cell media was discarded. The cells were washed with PBS three times, then harvested in 0.5 mL PBS. Samples were analyzed by flow cytometry with FACSDiva on a LSRII flow cytometer (BD Biosciences), and data were analyzed with FlowJo software.

Cell Fluorescence Measurements

RAW 264.7 cells were seeded in 1 mL of medium on a 12-well plate at 2×10^5 cells per well and cultured for 24 h. 10 μL of polymersomes (5 mg/mL in PBS) per well were added at desired time points (8, 24, 48 and 72 h before harvest). After incubation, cell media was discarded. The cells were washed with PBS three times, then harvested in 0.5 mL PBS. Samples were analyzed by Flow cytometry. Control cells were cultured in medium alone.

Animals

C57BL/6 male mice, 6–8 weeks old, were purchased from Jackson Laboratories. All mice were housed and maintained in the Center for Comparative Medicine at Northwestern University. All animal experimental procedures were performed according to protocols approved by the Northwestern University Institutional Animal Care and Use Committee (IACUC).

Subcutaneous Injections of Polymersomes in C57BL/6 Mice

Polymersomes composed of PEG_{17}-PPS_{28}-PBI-PPS_{28}-PEG_{17} and PEG_{17}-PPS_{28} (1/1) were prepared in

PBS at 10 mg/mL. C57BL/6 mice (n = 3) were injected subcutaneously on both sides of their back with 75 μL of polymersomes. Control mice were injected with PBS. At different time points (24, 48 and 72 h post-injection), animals were anesthetized by intraperitoneal (i.p.) injection of a mixture of Ketamine/Xylazine followed by exsanguination. Blood was collected by retro-orbital puncture with BD Microtainer tubes and dipotassium EDTA (BD Biosciences). Serum was separated by centrifugation at 3000 rpm at 4 °C for 25 min. To prepare white blood cell suspensions, blood cells were washed twice with 10 ml PBS and treated 3× with ammonium-chloride-potassium (ACK) lysis buffer (Invitrogen) to eliminate red blood cells. Brachial lymph nodes, spleen, and liver were harvested, gently dissociated and incubated in 2 ml of Collagenase D (2 mg/mL) on a 12-well plate for 45 min at 37 °C and 5% CO_2. Single-cell suspensions were prepared by mechanical dissociation and passing through a 70 μm cell strainer. Anti-mouse CD16/CD32 was used to block FcRs and Zombie Aqua fixable viability dye was used to determine live/dead cells. For flow cytometric analysis, cells were stained using cocktails of fluorophore-conjugated anti-mouse antibodies (Biolegend): panel 1: CD45-APC, CD3-APC/Cy7, CD49b- PerCP-Cy5.5, CD8α-PE/Cy7, CD19-Pacific Blue; panel 2: CD11c-Pacific Blue, CD8α-PE-Cy7, CD11b-PerCP-Cy5.5, CD45RB/B220-APC, Gr-1-APC-Cy7; and panel 3: F4/80-Pacific Blue, CD11c-APC, CD11b-PerCP-Cy5.5, Ly6C-APC/Cy7, Ly6G-PE/Cy7. After washes, cells were fixed by IC cell fixation buffer (Biosciences). Flow cytometry was performed with FACSDiva on a LSRII flow cytometer (BD Biosciences) and data were analyzed with FlowJo software.

RESULTS AND DISCUSSION

Synthesis and Characterization of PEG_{17}-PPS_{28}-PBI-PPS_{28}-PEG_{17}

Aggregation behavior of PEG-PPS di- and triblock copolymers has been reported previously.[4] A wide range of morphologies can be obtained by controlling the molecular weight ratio of the hydrophilic PEG fraction (f_{PEG}). Here, a novel tetrablock copolymer formed from two separate PEG-PPS diblock copolymers linked by a PBI bridge was designed for assembly into vesicular polymersome nanostructures. Our previous work has demonstrated that PEG_{17}-PPS_{30} can form uniform vesicle structures in aqueous solution,[4,36,38] and we utilized the same f_{PEG} to synthesize the tetrablock copolymer PEG_{17}-PPS_{28}-PBI-PPS_{28}-PEG_{17}. Scheme 1 illustrates the synthetic route for the amphiphilic tetrablock copolymer. To introduce an amino group at the end of the PEG_{17}-PPS_{28} diblock copolymer, *N*-(3-bromopropyl)phthalimide was used to terminate the PEG thioacetate initiated anionic ring opening polymerization of propylene sulfide. Then the amino end-functionalized PEG-PPS block copolymer (PEG-PPS-NH_2) was obtained by the removal of the phthaloyl group from *N*-(3-bromopropyl)phthalimide end-capped PEG-PPS block copolymer (PEG-PPS-PI) using a hydrazinolysis method in ethanol.[4] Finally PEG_{17}-PPS_{28}-PBI-PPS_{28}-PEG_{17} block copolymer was prepared by conjugation of PEG-PPS-NH_2 with PTCDA. The product of PEG-PPS-PBI-PPS-PEG was characterized by ^{1}H NMR spectroscopy and GPC, as shown in Fig. 2. The NMR characteristic signal at about 8.6 ppm was ascribed to the aromatic proton peaks of PBI, demonstrating that the fluorescent PBI group had been successfully conjugated to PEG-PPS. The GPC peak of PEG_{17}-PPS_{28}-PBI-PPS_{28}-PEG_{17} depicts a monomodal distribution of polymeric species and a clear shift to higher molecular weight compared with PEG_{17}-PPS_{28} diblock copolymer.

All subsequent experiments were performed using modular mixtures of the diblock and tetrablock copolymers. The copolymer mixture resulted in a shoulder peak on the GPC curve with an elution time identical to the pure diblock copolymer (Fig. 2b). There are two reasons why we used mixtures of the diblock and tetrablock for subsequent experiments. First, at high aggregate concentrations, π–π stacking of PBI results in fluorescence quenching.[42] Incorporation of the diblock therefore permits a detectable red emission to allow imaging of the intact assembled polymersomes. Second, since both the copolymers contain the same f_{PEG}, they will both assemble into vesicular nanostructures, which allows a modular approach to the formation of polymersome nanocarriers. While the tetrablock module imparts useful fluorescent properties, additional diblock modules may be used for the incorporation of targeting ligands or supplemental imaging modalities such as MRI contrast agents for multimodal imaging strategies.

Assembly and Characterization of Modular Tetrablock/Diblock Polymersomes

Stable polymersome solutions of PEG_{17}-PPS_{28}-PBI-PPS_{28}-PEG_{17}/PEG_{17}-PPS_{28} in PBS were successfully prepared using the thin film hydration method followed by extrusion through a 200 nm nylon filter. The cryoTEM image in Fig. 2c shows the representative size and morphology of the aggregates, which revealed that small polymersomes were formed with diameters between 20–50 nm. Assembled morphologies appeared to be greater than 99% vesicular, with an extremely

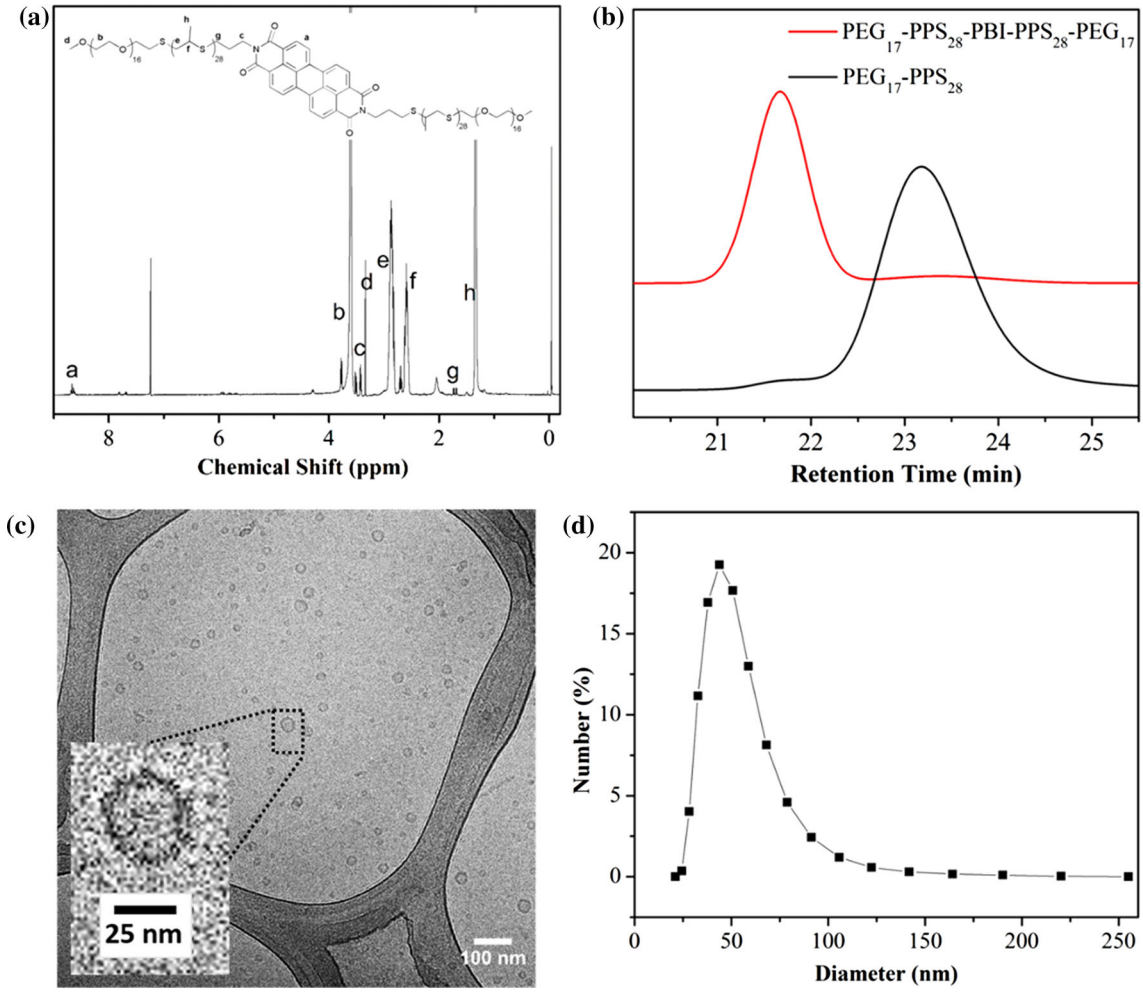

FIGURE 2. Characterization of tetrablock copolymer and resulting self-assembled polymersomes in phosphate buffered saline (PBS). (a) ^{1}H NMR spectrum of PEG_{17}-PPS_{28}-PBI-PPS_{28}-PEG_{17} in $CDCl_3$. (b) GPC traces of PEG_{17}-PPS_{28}-PBI-PPS_{28}-PEG_{17} and PEG_{17}-PPS_{28} copolymers. (c) CryoTEM image of 1:1 PEG_{17}-PPS_{28}-PBI-PPS_{28}-PEG_{17} : PEG_{17}-PPS_{28} polymersomes in PBS at a concentration of 10 mg/mL (scale bar = 100 nm). (d) Dynamic light scattering (DLS) measurement of the polymersome size distribution in PBS (1 mg/mL). The averaged diameter is 60 nm with PDI = 0.220.

small number (<1%) of micelles and filomicelles visible. The hydrodynamic size and size distributions of polymersome were further characterized by dynamic light scattering (DLS) (Fig. 2d). The intensity-average hydrodynamic diameter was evaluated to be 60 nm with a polydispersity index (PDI) of 0.22.

Polymersomes assembled solely from PEG_{17}-PPS_{28}-PBI-PPS_{28}-PEG_{17} exhibited a weak, concentration dependent and strongly quenched excimer-like red emission at 640 nm under UV illumination in PBS (Figs. 3a and S1a). As the percentage of the PEG_{17}-PPS_{28} diblock increased within modular assemblies, the intensity of the red fluorescence increased, with a maximum signal detected at a 1:1 ratio (Fig. 3a). The intensity decreased after further increasing the diblock percentage beyond 57%, but the fluorescence intensity ratio at 550 nm and 640 nm ($I_{550/640}$) remained constant at approximately 0.5 regardless of the triblock/diblock ratio (Fig. 3b). Micelles composed of PEG-PBI that have a PBI hydrophobic core do not demonstrate the red shift that we observed here.[18] This suggests that placing PBI between two highly hydrophobic PPS blocks enhances the ability for PBI to participate in π-stacking. But as the PEG-*bl*-PPS diblock percentage increased, the density of PBI decreased, potentially decreasing the opportunity for PBI molecules to come into contact and participate in π–π stacking.

Modular Polymersomes Containing PEG_{17}-PPS_{28}-PBI-PPS_{28}-PEG_{17} Tetrablocks Undergo a Red to Green Emission Shift upon Oxidation with Biologically Relevant Levels of ROS

If flanking PBI with two hydrophobic PPS blocks enhances PBI π-stacking and red emission, we

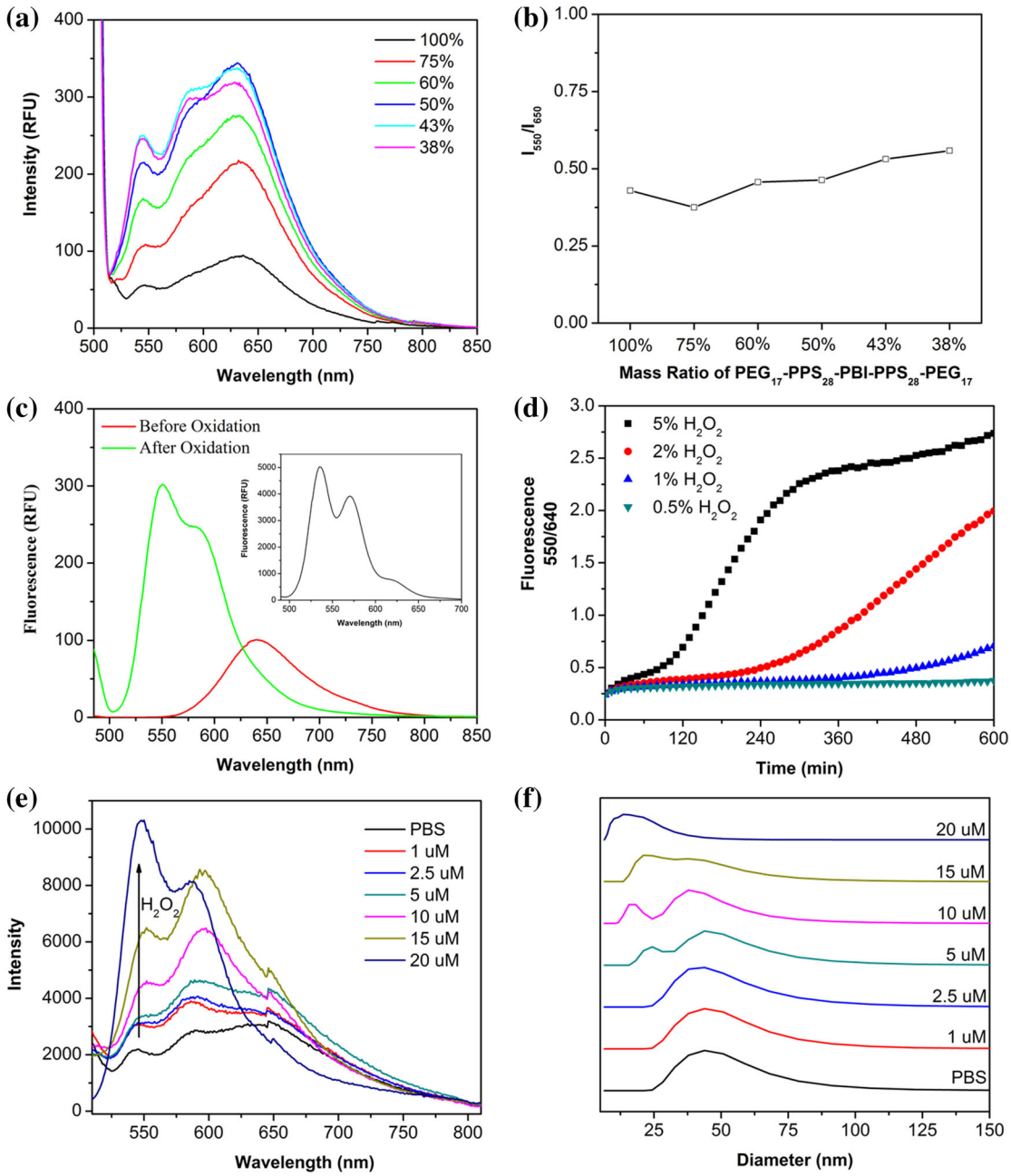

FIGURE 3. Characterization of PEG_{17}-PPS_{28}-PBI-PPS_{28}-PEG_{17} polymersome spectral properties. (a) Red fluorescence emission and (b) red/green emission intensity ratio of polymersomes composed of different ratios of PEG_{17}-PPS_{28}-PBI-PPS_{28}-PEG_{17} and PEG_{17}-PPS_{28}. The percentage of tetrablock in each tested formulation is shown in the legend. (c) Fluorescence spectra of polymersomes in PBS (2 mg/mL) before and after oxidation by H_2O_2. The emission in DCM (2 mg/mL) is inserted into the top right corner of the image. (d) Plots of fluorescence intensity ratio at 550 nm and 640 nm as a function of the incubation time at various H_2O_2 concentrations at 37 °C. RFU = relative fluorescence unit, λ_{ex} = 485 nm. (e) Emission spectra and (f) vesicle-to-micelle transition of 100% PEG_{17}-PPS_{28}-PBI-PPS_{28}-PEG_{17} polymersomes after reaction with physiological concentrations of H_2O_2. Micelle formation was monitored by DLS.

hypothesized that increasing the hydrophilicity of the neighboring PPS blocks may disrupt PBI π-stacking and shift the fluorescence towards a green emission. PPS oxidizes into the progressively more hydrophilic variants poly(propylene sulfoxide) and poly(propylene sulfone).[31,38] In consideration of this oxidation sensitivity, we expected that polymersomes containing PEG_{17}-PPS_{28}-PBI-PPS_{28}-PEG_{17} tetrablocks would

exhibit a fluorescence shift during oxidation-dependent disassembly by disrupting the π–π stacking of PBI aggregates within their membranes. Oxidation of PPS within PEG-*bl*-PPS polymersome by H_2O_2 results in reassembly of the vesicular nanostructure into smaller solid core spherical micelles, which can be monitored by decreases in both nanoparticle size as detected by DLS and turbidity of the solution as measured by optical absorbance.[38] After oxidation of the milky polymersome dispersion with H_2O_2 to form an optically clear solution, the red fluorescence peak at 640 nm shifted to a strong green emission at 550 nm (Fig. 3c). This green emission compared well with the emission in organic solvent of the completely solubilized tetrablock copolymer (Fig. 3c insert). We further investigated the response speed at 37 °C with various H_2O_2 concentrations (0.5, 1, 2, and 5%) by evaluating the $I_{550/640}$ ratio (Fig. 3d). The results revealed a quantifiable response that was sensitive to the concentration of H_2O_2. Disruption of PBI π–π stacking to generate a shift in the $I_{550/640}$ ratio occurred after 50 h using a 5% H_2O_2 concentration. This minimalist *in vitro* experiment verifies sensitivity of the polymersome fluorescence to ROS, but it should be noted that *in vivo* these shifts in $I_{550/640}$ ratio may vary extensively by cell type, activation state, and mechanism of endocytosis due to the dynamic and complex mixtures of ROS present in endosomal compartments.[1,2,7,34,35]

To investigate oxidation of PEG-*bl*-PPS copolymers at intracellular ROS concentrations, which are typically below 100 μM,[25] we monitored the shift in fluorescence for polymersomes incubated with H_2O_2 concentrations between 1 and 20 μM (Fig. 3e). The emission spectrum of polymersomes at each concentration was measured until the fluorescence stabilized to indicate that the maximum level of oxidation had been achieved. The minimal H_2O_2 concentration required for sufficient oxidation to disrupt PBI π–π stacking was found to be 20 μM, which required 3 weeks to achieve. We additionally used DLS to monitor the vesicle-to-micelle transition that occurs during PEG-*bl*-PPS polymersome oxidation at these same physiologically relevant ROS concentrations (Fig. 3f). We observed micelles at 5 μM and above concentrations of H_2O_2. On a molar basis, 5 μM would correspond to a theoretical 25% oxidation of all available PPS units, and this corresponds well with previously published results demonstrating that a 20% oxidation of PPS is required for the vesicle-to-micelle transition.[38] Furthermore, 20 μM H_2O_2 was required for complete conversion of all vesicles into micelles, and this corresponded to the oxidation level necessary for the red to green fluorescence shift (Fig. 3e).

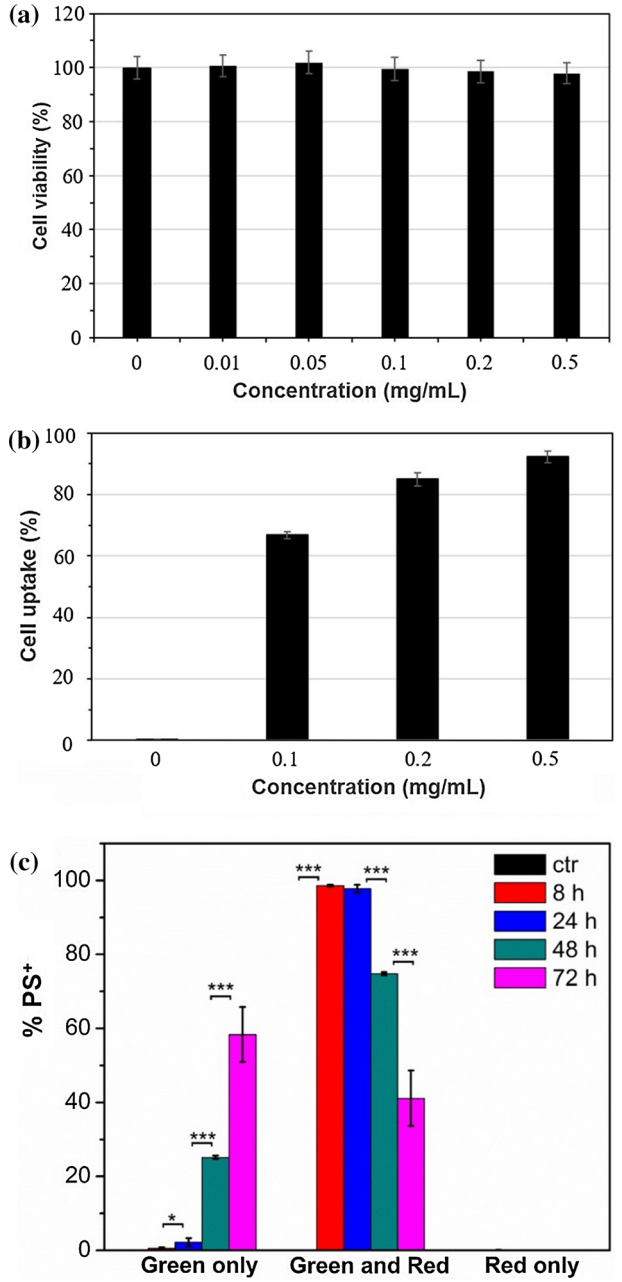

FIGURE 4. ***In vitro*** **characterization of PEG_{17}-PPS_{28}-PBI-PPS_{28}-PEG_{17} polymersomes with RAW 264.7 macrophages. (a) Cytotoxicity of polymersomes after a 48 h incubation with cells. (b) Cellular uptake of polymersomes after a 3 h incubation with cells. (c) Intracellular fluorescence change of polymersome positive (PS^+) cells following endocytosis of polymersomes at 50 μg/mL at different time points. PBS was added to control (ctr) cells instead of polymersomes. Statistical significance: *$p \leq 0.1$; **$p \leq 0.05$; ***$p \leq 0.001$.**

In Vitro Toxicity and Cellular Uptake of Modular Tetrablock/Diblock Polymersomes

Based on the demonstrated optimal fluorescence emission discussed above, polymersomes composed of a 1:1 ratio of tetrablock : diblock were selected for

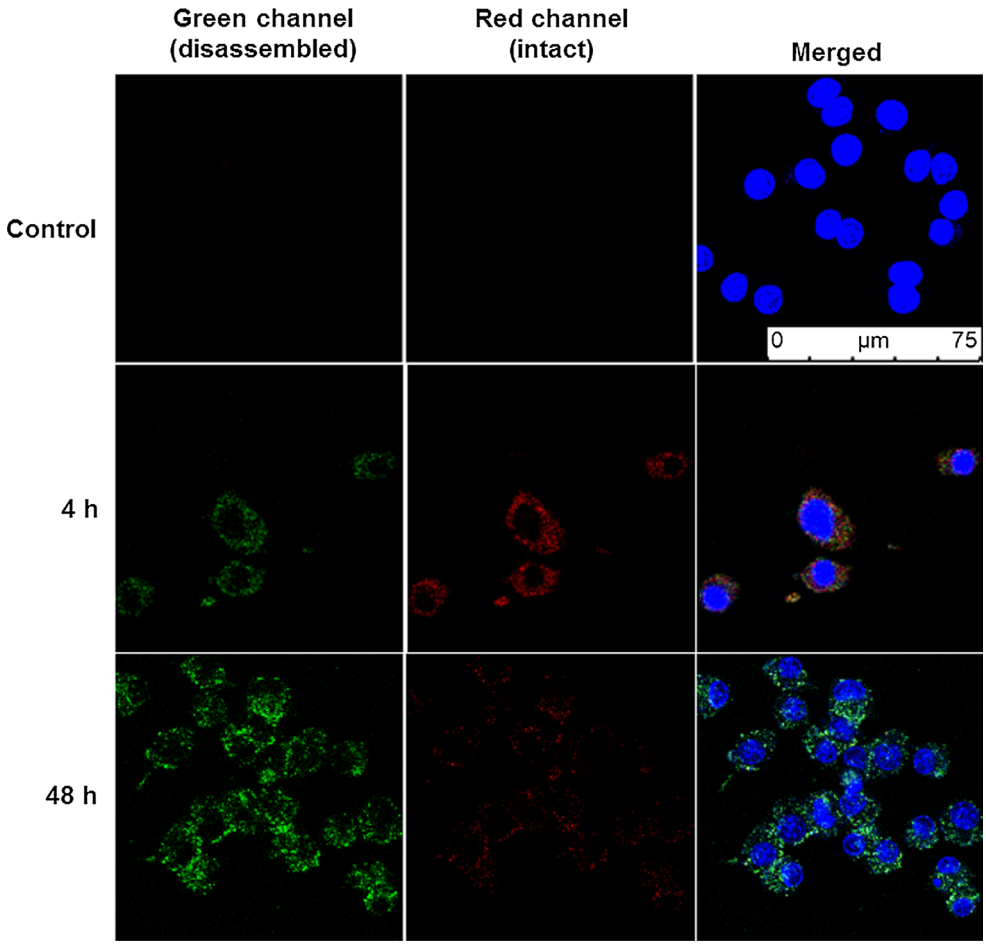

FIGURE 5. Confocal microscopy of PEG_{17}-PPS_{28}-PBI-PPS_{28}-PEG_{17} polymersomes within RAW 264.7 macrophages. Cells were incubated with polymersomes for 4 h, washed with fresh media to remove polymersomes that had not been endocytosed and subsequently imaged at timepoints of 4 h and 48 h. Control samples were incubated for 48 h in media without polymersomes.

subsequent *in vitro* and *in vivo* investigations. A cell viability assay using RAW 264.7 macrophages incubated for 48 h with a range of polymersome concentrations up to 0.5 mg/mL revealed no detectable toxicity (Fig. 4a). Uptake of polymersomes by RAW 264.7 macrophages increased with concentration as measured by flow cytometry, and approximately 95% of cells were positive for polymersomes (PS^+) after a 3 h incubation at 0.5 mg/mL (Fig. 4b). The percentages of cells that were positive for red verses green fluorescence was monitored over the course of 72 h (Fig. 4c). By 8 h, nearly 100% of observed macrophages displayed a mixture of red and green fluorescence. Over the next 60 h, the percentages of cells that were positive only for green fluorescence increased significantly, indicating a consistent intracellular disassembly of polymersomes. At no time were any cells found to be positive solely for the red channel, which reflected the rapid endosomal degradation known to occur in macrophages at early stages of phagocytosis. These results were further verified by confocal microscopy (Fig. 5). Images revealed all visible cells to contain both red and green fluorescence after 4 h of incubation with polymersomes, with most endosomes displaying the red emission associated with intact vesicles. By the 48 h time point, no endosomes could be observed to possess only red fluorescence. Instead, the vast majority displayed either a green emission or a yellow color when the channels were overlaid, which is indicative of endosomes containing increasing amounts of disassembled polymersomes lacking π-stacked PBI.

In Vivo Detection of Polymersome Disassembly Within Lymph Node Resident Phagocytes

To assess the detection of polymersome disassembly under oxidative conditions within phagocytic cells *in vivo*, 1:1 tetrablock/diblock polymersomes were injected SC into the backs of mice. The draining

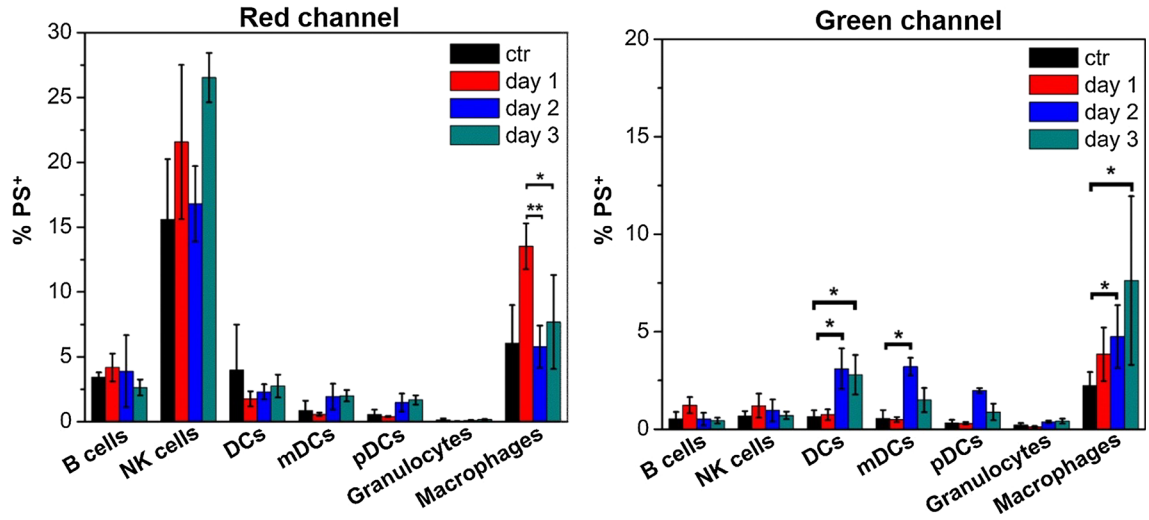

FIGURE 6. ***In vivo*** **monitoring of PEG_{17}-PPS_{28}-PBI-PPS_{28}-PEG_{17} polymersome disassembly within lymph node resident immune cell populations. Polymersomes (10 mg/mL) or PBS controls (ctr) were injected subcutaneously into mice and brachial lymph nodes were extracted at the indicated time points for analysis by flow cytometry. Histograms show the average percentages ± standard deviation of polymersome positive (PS^+) cells for each indicated cell type. Macrophages: $CD11b^+F4/80^+$; dendritic cells (DCs): $CD11c^+$; mature DCs (mDCs): $I\text{-}A/I\text{-}E^+CD11c^+$; plasmacytoid DCs (pDCs): $I\text{-}A/I\text{-}E^+CD11c^+Gr\text{-}1^+B220^+$; B cells: $CD45^+CD19^+$; natural killer (NK) cells: $CD45^+CD49b^+$; granulocytes: $Gr\text{-}1^+CD11b^+$. Statistical significance: $^*p \le 0.1$; $^{**}p \le 0.05$; $^{***}p \le 0.001$.**

brachial lymph nodes were extracted at time points ranging from 1 to 3 days, and resident cells were analyzed by flow cytometry for red and green channel emissions, which respectively corresponded to intact and disassembled polymersomes (Figs. 6 and S2). Natural killer (NK) cells and macrophages were found to have a strong association with intact polymersomes at all time points. NK cells are not highly phagocytic, except under unique occasions,[39] and this is supported by their 550 emission. No detectable 550 emission was observed over the course of three days, suggesting that polymersomes associating with NK cells were not disassembling and likely not endocytosed. It is possible that an NK cell surface receptor was capable of binding to motifs within the adsorbed protein corona of the polymersomes. Such association would not result in polymersome disassembly, and these results demonstrate the benefit of identifying not just cells associating with nanocarriers, but specifically which cells received intracellular delivery of payloads. On the contrary, the number of macrophages displaying a strong 550 emission progressively increased over time. This trend mirrored the fluorescence shift that was observed over the same time course during the *in vitro* RAW 264.7 macrophage experiments (Fig. 4c). The highest uptake of intact polymersomes occurred on day 1, when approximately 15% of macrophages were positive for polymersomes. A significant increase in 550 emission was observed on day 2 and continued to increase into day 3 when over 10% of isolated macrophages contained disassembled polymersomes. Surprisingly, DCs did not display a significant increase in 640 emission on any day, but did show significant increases in 550 emission on day 2. These green emissions appeared to plateau on day 2, as day 3 did not reveal a further significant increase in polymersome disassembly as was observed for macrophages. Considered the most potent professional APC, DCs have separate immunological roles than macrophages as well as distinct mechanisms of endosomal alkylation and ROS generation.[17,34,35] Furthermore, DCs have been found to increase their ROS generation and proteolysis phagocytosed materials following activation of their toll-like-receptors (TLRs).[40,41] PEG-*bl*-PPS nanocarriers are nonimmunogenic and do not elicit inflammatory responses unless transporting immunostimulatory payloads.[36,37] The lower levels of polymersome degradation by DCs may therefore reflect their more selective mechanisms of ROS generation compared to macrophages, which are instead constitutively collecting and destroying extracellular debris to fulfil their role as the professional "garbage collectors" of the immune system.[11,12]

CONCLUSIONS

An immunotheranostic nanocarrier system may lead to improved understanding of how the immune system functions as well as the rational design of

immunotherapeutic strategies. Here, we have characterized *in vitro* and *in vivo* a polymersome platform that employs modularly assembled tetrablock/diblock copolymers that allow fluorescence-based detection of intracellular oxidation and nanocarrier disassembly. Polymersomes assembled from a 1:1 ratio of PEG_{17}-PPS_{28}-PBI-PPS_{28}-PEG_{17} : PEG_{17}-PPS_{28} allowed assessment of the time course of their degradation based upon the oxidation-induced disruption of PBI π–π stacking. We verified that diblock and tetrablock copolymers could be modularly assembled into stable vesicles, as reflected by the continued disruption of π–π stacking within assembled PEG_{17}-PPS_{28}-PBI-PPS_{28}-PEG_{17} membranes with increasing incorporation of PEG_{17}-PPS_{28}. A shift from red to green fluorescence was observed at physiologically relevant concentrations of ROS, and this was reproduced within the endosomal compartments of macrophages *in vitro* following uptake of modular polymersomes. *In vivo*, non-specific membrane association of polymersomes with cell surfaces could be separated from intracellular delivery, and both macrophages and DCs were found to continue to process and degrade polymersomes over 3 days after an initial subcutaneous injection. Future applications of this nanocarrier system include the identification of key cell populations targeted and activated by different vaccine formulations, the investigation of how specific combinations of TLR stimulation enhance DC function, as well as a wide range of strategies that may help unravel the complexities of immune responses.

ELECTRONIC SUPPLEMENTARY MATERIAL

The online version of this article (doi:10.1007/s12195-017-0486-7) contains supplementary material, which is available to authorized users.

ACKNOWLEDGMENTS

We would like to thank J. Remis for CryoTEM assistance and the following facilities at Northwestern University: Robert H. Lurie Comprehensive Cancer Center Flow Cytometry Core; Center for Advanced Molecular Imaging; Biological imaging facility; Mouse Histology and Phenotyping Laboratory; and the Keck Interdisciplinary Surface Science Facility. This work was supported by the National Institutes of Health Director's New Innovator Award (grant no. 1DP2HL132390-01), the Louis A. Simpson & Kimberly K. Querrey Center for Regenerative Nanomedicine Regenerative Nanomedicine Catalyst Award.

CONFLICT OF INTEREST

Fanfan Du, Yu-Gang Liu, and Evan A. Scott declare that they have no conflicts of interest.

ETHICAL STANDARDS

No human studies were carried out by the authors for this article. All institutional and national guidelines for the care and use of laboratory animals were followed and approved by the Northwestern University Institutional Animal Care and Use Committee.

REFERENCES

[1]Belizaire, R., and E. R. Unanue. Targeting proteins to distinct subcellular compartments reveals unique requirements for MHC class I and II presentation. *Proc Natl. Acad. Sci. U.S.A.* 106(41):17463–17468, 2009. doi:10.1073/pnas.0908583106.

[2]Berton, G., P. Bellavite, G. de Nicola, P. Dri, and F. Rossi. Plasma membrane and phagosome localisation of the activated NADPH oxidase in elicited peritoneal macrophages of the guinea-pig. *J. Pathol.* 136(3):241–252, 1982. doi:10.1002/path.1711360307.

[3]Blander, J. M., and R. Medzhitov. On regulation of phagosome maturation and antigen presentation. *Nat. Immunol.* 7(10):1029–1035, 2006. doi:10.1038/ni1006-1029.

[4]Cerritelli, S., C. P. O'Neil, D. Velluto, A. Fontana, M. Adrian, J. Dubochet, and J. A. Hubbell. Aggregation behavior of poly(ethylene glycol-bl-propylene sulfide) di- and triblock copolymers in aqueous solution. *Langmuir* 25(19):11328–11335, 2009. doi:10.1021/la900649m.

[5]Chen, Z., V. Stepanenko, V. Dehm, P. Prins, L. D. Siebbeles, J. Seibt, P. Marquetand, V. Engel, and F. Wurthner. Photoluminescence and conductivity of self-assembled pi–pi stacks of perylene bisimide dyes. *Chemistry* 13(2):436–449, 2007. doi:10.1002/chem.200600889.

[6]Cohn, L., and L. Delamarre. *Dendritic cell-targeted vaccines. Front Immunol.* 5:255, 2014. doi:10.3389/fimmu.2014.00255.

[7]Delamarre, L., M. Pack, H. Chang, I. Mellman, and E. S. Trombetta. Differential lysosomal proteolysis in antigen-presenting cells determines antigen fate. *Science* 307(5715):1630–1634, 2005. doi:10.1126/science.1108003.

[8]Dexter, D. L., H. M. Kowalski, B. A. Blazar, Z. Fligiel, R. Vogel, and G. H. Heppner. Heterogeneity of tumor cells from a single mouse mammary tumor. *Cancer Res.* 38(10):3174–3181, 1978.

[9]Dowling, D. J., E. A. Scott, A. Scheid, I. Bergelson, S. Joshi, C. Pietrasanta, S. Brightman, G. Sanchez-Schmitz, S. D. Van Haren, J. Ninkovic, D. Kats, C. Guiducci, A. de Titta, D. K. Bonner, S. Hirosue, M. A. Swartz, J. A. Hubbell, O. Levy. Toll-like receptor 8 agonist nanoparticles mimic immunomodulating effects of the live BCG vaccine and enhance neonatal innate and adaptive immune responses. *J. Allergy Clin. Immunol.* 2017. doi:10.1016/j.jaci.2016.12.985.

[10]Du, F. F., J. Tian, H. Wang, B. Liu, B. K. Jin, and R. K. Bai. Synthesis and luminescence of POSS-containing perylene bisimide-bridged amphiphilic polymers. *Macromolecules* 45(7):3086–3093, 2012. doi:10.1021/ma300100s.

[11]Elliott, M. R., K. M. Koster, and P. S. Murphy. Efferocytosis signaling in the regulation of macrophage inflammatory responses. *J. Immunol.* 198(4):1387–1394, 2017. doi:10.4049/jimmunol.1601520.
[12]Elliott, M. R., and K. S. Ravichandran. Clearance of apoptotic cells: implications in health and disease. *J. Cell Biol.* 189(7):1059–1070, 2010. doi:10.1083/jcb.201004096.
[13]Gray, E. E., and J. G. Cyster. Lymph node macrophages. *J Innate Immun.* 4(5–6):424–436, 2012. doi:10.1159/000337007.
[14]Gupta, M. K., T. A. Meyer, C. E. Nelson, and C. L. Duvall. Poly(PS-b-DMA) micelles for reactive oxygen species triggered drug release. *J. Control. Release* 162(3):591–598, 2012. doi:10.1016/j.jconrel.2012.07.042.
[15]Gvishi, R., and R. Reisfeld. New stable tunable solid-state dye-laser in the red. *Optoelectron. Appl. Ind. Med.* 1972:390–399, 1993. doi:10.1117/12.151121.
[16]Gvishi, R., R. Reisfeld, and Z. Burshtein. Spectroscopy and laser action of the red perylimide dye in various solvents. *Chem. Phys. Lett.* 213(3–4):338–344, 1993. doi:10.1016/0009-2614(93)85142-B.
[17]Joffre, O. P., E. Segura, A. Savina, and S. Amigorena. Cross-presentation by dendritic cells. *Nat. Rev. Immunol.* 12(8):557–569, 2012.
[18]Jouault, N., Y. J. Xiang, E. Moulin, G. Fuks, N. Giuseppone, and E. Buhler. Hierarchical supramolecular structuring and dynamical properties of water soluble polyethylene glycol-perylene self-assemblies. *PCCP* 14(16):5718–5728, 2012. doi:10.1039/c2cp23786e.
[19]Kaiser, T. E., H. Wang, V. Stepanenko, and F. Wurthner. Supramolecular construction of fluorescent J-aggregates based on hydrogen-bonded perylene dyes. *Angew. Chem. Int. Ed. Engl.* 46(29):5541–5544, 2007. doi:10.1002/anie.200701139.
[20]Kelkar, S. S., and T. M. Reineke. Theranostics: combining imaging and therapy. *Bioconj Chem.* 22(10):1879–1903, 2011. doi:10.1021/bc200151q.
[21]Klebe, G., F. Graser, E. Hadicke, and J. Berndt. Crystallochromy as a solid-state effect—correlation of molecular-conformation, crystal packing and color in perylene-3,4-9,10-bis(dicarboximide) pigments. *Acta Crystallogr. B* 45:69–77, 1989. doi:10.1107/S0108768188010407.
[22]Langhals, H., S. Demmig, and T. Potrawa. The relation between packing effects and solid-state fluorescence of dyes. *J. Prakt. Chem.* 333(5):733–748, 1991. doi:10.1002/prac.19913330508.
[23]Langhals, H., W. Jona, F. Einsiedl, and S. Wohnlich. Self-dispersion: spontaneous formation of colloidal dyes in water. *Adv. Mater.* 10(13):1022–1024, 1998. doi:10.1002/(Sici)1521-4095(199809)10:13<1022::Aid-Adma1022>3.3.Co;2-F.
[24]Lennon-Dumenil, A. M., A. H. Bakker, R. Maehr, E. Fiebiger, H. S. Overkleeft, M. Rosemblatt, H. L. Ploegh, and C. Lagaudriere-Gesbert. Analysis of protease activity in live antigen-presenting cells shows regulation of the phagosomal proteolytic contents during dendritic cell activation. *J. Exp. Med.* 196(4):529–540, 2002.
[25]Li, T. S., and E. Marban. Physiological levels of reactive oxygen species are required to maintain genomic stability in stem cells. *Stem Cells* 28(7):1178–1185, 2010. doi:10.1002/stem.438.
[26]Lim, E. K., T. Kim, S. Paik, S. Haam, Y. M. Huh, and K. Lee. Nanomaterials for theranostics: recent advances and future challenges. *Chem. Rev.* 115(1):327–394, 2015.
[27]Lukacs, G. L., O. D. Rotstein, and S. Grinstein. Phagosomal acidification is mediated by a vacuolar-type H(+)-ATPase in murine macrophages. *J. Biol. Chem.* 265(34):21099–21107, 1990.
[28]Lukacs, G. L., O. D. Rotstein, and S. Grinstein. Determinants of the phagosomal pH in macrophages. In situ assessment of vacuolar H(+)-ATPase activity, counterion conductance, and H+ "leak". *J. Biol. Chem.* 266(36):24540–24548, 1991.
[29]Mais, S., J. Tittel, T. Basche, C. Brauchle, W. Gohde, H. Fuchs, G. Muller, and K. Mullen. Terrylenediimide: a novel fluorophore for single-molecule spectroscopy and microscopy from 1.4 K to room temperature. *J. Phys. Chem. A* 101(45):8435–8440, 1997. doi:10.1021/jp9719063.
[30]Napoli, A., M. J. Boerakker, N. Tirelli, R. J. M. Nolte, N. A. J. M. Sommerdijk, and J. A. Hubbell. Glucose-oxidase based self-destructing polymeric vesicles. *Langmuir* 20(9):3487–3491, 2004. doi:10.1021/La0357054.
[31]Napoli, A., M. Valentini, N. Tirelli, M. Muller, and J. A. Hubbell. Oxidation-responsive polymeric vesicles. *Nat. Mater.* 3(3):183–189, 2004. doi:10.1038/nmat1081.
[32]Parker, J. S., and C. M. Perou. Tumor heterogeneity: focus on the leaves, the trees, or the forest? *Cancer Cell* 28(2):149–150, 2015. doi:10.1016/j.ccell.2015.07.011.
[33]Postow, M. A., J. Chesney, A. C. Pavlick, C. Robert, K. Grossmann, D. McDermott, G. P. Linette, N. Meyer, J. K. Giguere, S. S. Agarwala, M. Shaheen, M. S. Ernstoff, D. Minor, A. K. Salama, M. Taylor, P. A. Ott, L. M. Rollin, C. Horak, P. Gagnier, J. D. Wolchok, and F. S. Hodi. Nivolumab and ipilimumab versus ipilimumab in untreated melanoma. *N. Engl. J. Med.* 372(21):2006–2017, 2015. doi:10.1056/NEJMoa1414428.
[34]Savina, A., and S. Amigorena. Phagocytosis and antigen presentation in dendritic cells. *Immunol. Rev.* 219:143–156, 2007. doi:10.1111/j.1600-065X.2007.00552.x.
[35]Savina, A., C. Jancic, S. Hugues, P. Guermonprez, P. Vargas, I. C. Moura, A. M. Lennon-Dumenil, M. C. Seabra, G. Raposo, and S. Amigorena. NOX2 controls phagosomal pH to regulate antigen processing during crosspresentation by dendritic cells. *Cell* 126(1):205–218, 2006. doi:10.1016/j.cell.2006.05.035.
[36]Scott, E. A., A. Stano, M. Gillard, A. C. Maio-Liu, M. A. Swartz, and J. A. Hubbell. Dendritic cell activation and T cell priming with adjuvant- and antigen-loaded oxidation-sensitive polymersomes. *Biomaterials* 33(26):6211–6219, 2012. doi:10.1016/j.biomaterials.2012.04.060.
[37]Stano, A., E. A. Scott, K. Y. Dane, M. A. Swartz, and J. A. Hubbell. Tunable T cell immunity towards a protein antigen using polymersomes vs. solid-core nanoparticles. *Biomaterials* 34(17):4339–4346, 2013. doi:10.1016/j.biomaterials.2013.02.024.
[38]Vasdekis, A. E., E. A. Scott, C. P. O'Neil, D. Psaltis, and J. A. Hubbell. Precision intracellular delivery based on optofluidic polymersome rupture. *ACS Nano* 6(9):7850–7857, 2012. doi:10.1021/nn302122h.
[39]Voigt, J., K. Hunniger, M. Bouzani, I. D. Jacobsen, D. Barz, B. Hube, J. Loffler, and O. Kurzai. Human natural killer cells acting as phagocytes against *Candida albicans* and mounting an inflammatory response that modulates neutrophil antifungal activity. *J. Infect. Dis.* 209(4):616–626, 2014. doi:10.1093/infdis/jit574.
[40]Vulcano, M., S. Dusi, D. Lissandrini, R. Badolato, P. Mazzi, E. Riboldi, E. Borroni, A. Calleri, M. Donini, A. Plebani, L. Notarangelo, T. Musso, and S. Sozzani. Toll

receptor-mediated regulation of NADPH oxidase in human dendritic cells. *J. Immunol.* 173(9):5749–5756, 2004.
[41]Wagner, C. S., J. Grotzke, and P. Cresswell. Intracellular regulation of cross-presentation during dendritic cell maturation. *PLoS ONE* 8(10):e76801, 2013. doi:10.1371/journal.pone.0076801.
[42]Wurthner, F. Perylene bisimide dyes as versatile building blocks for functional supramolecular architectures. *Chem. Commun.* 14:1564–1579, 2004. doi:10.1039/b401630k.
[43]Würthner, F., C. Bauer, V. Stepanenko, and S. Yagai. A black perylene bisimide super gelator with an unexpected J-type absorption band. *Adv. Mater.* 20(9):1695–1698, 2008. doi:10.1002/adma.200702935.
[44]Yamaguchi, T., and M. Kaneda. Presence of cytochrome b-558 in guinea-pig alveolar macrophages-subcellular localization and relationship with NADPH oxidase. *Biochim. Biophys. Acta* 933(3):450–459, 1988.
[45]Yi, S., S. D. Allen, Y. G. Liu, B. Z. Ouyang, X. Li, P. Augsornworawat, E. B. Thorp, and E. A. Scott. Tailoring nanostructure morphology for enhanced targeting of dendritic cells in atherosclerosis. *ACS Nano* 10(12):11290–11303, 2016. doi:10.1021/acsnano.6b06451.
[46]Zhang, X., Z. Chen, and F. Wurthner. Morphology control of fluorescent nanoaggregates by co-self-assembly of wedge- and dumbbell-shaped amphiphilic perylene bisimides. *J. Am. Chem. Soc.* 129(16):4886–4887, 2007. doi:10.1021/ja070994u.